

TASEP on parallel tracks: effects of mobile bottlenecks in fixed segments

Sumit Sinha and Debashish Chowdhury*

Department of Physics, Indian Institute of Technology, Kanpur 208016, India

We study the flux of totally asymmetric simple exclusion processes (TASEPs) on a twin co-axial square tracks. In this biologically motivated model the particles in each track act as mobile bottlenecks against the movement of the particles in the other although the particles are not allowed to move out of their respective tracks. So far as the outer track is concerned, the particles on the inner track act as bottlenecks only over a set of fixed segments of the outer track, in contrast to site-associated and particle-associated quenched randomness in the earlier models of disordered TASEP. In a special limiting situation the movement of particles in the outer track mimic a TASEP with a “point-like” immobile (i.e., quenched) defect where phase segregation of the particles is known to take place. The length of the inner track as well as the strength and number density of the mobile bottlenecks moving on it are the control parameters that determine the nature of spatio-temporal organization of particles on the outer track. Variation of these control parameters allow variation of the width of the phase-coexistence region on the flux-density plane of the outer track. Some of these phenomena are likely to survive even in the future extensions intended for studying traffic-like collective phenomena of polymerase motors on double-stranded DNA.

I. INTRODUCTION

Totally asymmetric simple exclusion process (TASEP) is one of the simplest models of non-equilibrium systems of interacting self-driven particles [1]. Properties of TASEP and its various extensions have been analyzed to get insight into the spatio-temporal organization in wide varieties of physical and biological systems [2–6]. In the simplest version of this model particles hop forward, with rate p , from one site to the next on a one-dimensional lattice of equi-spaced sites; however, a particle successfully executes the forward hop if, and only if, the target site is empty.

Effects of two types of quenched (time-independent) defects on the spatio-temporal organization of the particles have been explored extensively [2, 3]. (A) In one class of models of quenched defect the randomness is associated with the *lattice*: particles hop at the rate p from all sites except from the “point defect” from where the hopping rate is $p' < p$. Such a single defect site can give rise to a nontrivial macroscopic phase segregation of the particles into high-density and low-density regions [7]. Two types of extensions of this model have been reported: (i) $r (> 1)$ successive sites are occupied by defects so that the defect may be regarded as a single extended object of length r ; (ii) $r (> 1)$ point defects are distributed randomly over the entire lattice [8, 9] so that the lattice can be viewed as “disordered” rather than merely defective. In the latter case time-independent random hopping rates, drawn from a probability distribution $P(p)$, are assigned to each lattice site. From now onwards we refer to this class of models as random-site TASEP (RST). (B) In the second class of models with quenched defect, the randomness is associated with the particles: a single “impurity” particle is allowed to hop at a rate $p' < p$ whereas the hopping

rate of all the other particles is p . The growth of platoons of particles behind the impurity is reminiscent of coarsening phenomena and the steady state of the system can be expressed formally in terms of a Bose-Einstein-like condensate of the vacancies (absence of particles) in front of the impurity particle [10–12]. In the more general version of this model the particles are assigned time-independent hopping rates randomly drawn from a probability distribution [10–13]. From now onwards we refer to this class of models as random-particle TASEP (RPT).

In this paper we introduce a biologically-motivated quasi-one dimensional TASEP with two parallel tracks of lattice sites. Although the particles are not allowed to shift from one track to the other, the flow in each influences that in the other through a prescription that we define in the next section. We shall refer to this model as TASEP with mobile bottlenecks (TMB). As we’ll explain in the next section, in one special limit this TMB reduces to RST. We also indicate possible extensions of the model for potential applications in traffic-like collective phenomena in biological systems [5, 6]. Using a combination of approximate analytical arguments and highly accurate numerical simulations, we demonstrate the rich varieties of spatio-temporal organizations, including phase segregations, in this model.

II. THE MODEL AND ITS COMPARISON WITH OTHER MODELS OF DISORDERED TASEP

Dynamic blockage against directed (albeit stochastic) movement of proteins and macromolecular complexes along filamentous tracks is well known [6]. For example, a class of molecular motors walk along the surface of stiff tubular filaments called microtubules [6, 14]. Microtubule-associated proteins, which act as blockage against the forward stepping of these motors, can detach from the microtubule thereby opening up the blockage.

*Corresponding author: debch@iitk.ac.in

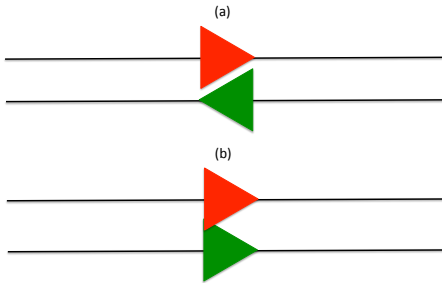


FIG. 1: (Color online) A schematic representation of the (a) head-on and (b) co-directional encounter of two polymerase motors moving along the two strands of a double-stranded DNA.

Similarly, several different types of molecular motors that walk along DNA or RNA strands face hindrance caused by proteins bound to the respective tracks [6]. Often these bound proteins either slide along the same track diffusively or, occasionally, detach from the track itself. Thus, most of the blockages against the movement of molecular motors are dynamic in nature. Our generic model here has been motivated by molecular motor traffic on DNA strands [15] which began receiving serious attention after Brewer [16] summarized the earlier experimental observations scattered in the literature. During DNA replication, the replication machine, called DNA polymerase (DNAP) moves along one of the two strands of a double-stranded DNA that serves as its track. During the same period another class of machines, called RNA polymerase (RNAP) transcribes the DNA. Often a DNAP and a RNAP approach each other head-on along the two strands of the double stranded DNA. Because of the close proximity of the two tracks, each acts as a dynamic blockage for the other. The model developed here is motivated by such traffic-like collective movement of particles on two parallel tracks (see fig.2).

Our model is shown schematically in Fig.2. It consists of two square tracks with a common center where the outer and inner tracks are labelled by the symbols T_o (outer) and T_i (inner), respectively. Each track consists of equi-spaced discrete sites; the lengths of the outer and inner tracks, denoted by L_o and L_i , respectively, are the total number of sites of the respective tracks. Particles on both tracks have identical size and each covers r consecutive lattice sites simultaneously (For $r > 1$, it might be more appropriate to regard these particles as hard rods). The number of particles on T_i and T_o are N_i and N_o , respectively; the corresponding *number densities* being $N_i/L_i = \rho_i$ and $N_o/L_o = \rho_o$, respectively. We also define the *coverage densities* $\rho_i^{cov} = r N_i/L_i$ and

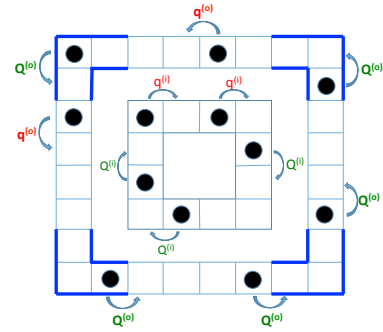


FIG. 2: (Color online) A schematic description of our model. The particles, represented by the black discs, on the outer lane hop unidirectionally with the probabilities $Q^{(o)}$ and $q^{(o)}$ per unit time in the absence and presence, respectively, of any hindering particle on the inner track. Similarly, the particles, also represented by the black discs, on the inner lane hop with the probabilities $Q^{(i)}$ and $q^{(i)}$ per unit time in the absence and presence, respectively, of any hindering particle on the outer track. No more than one particle can occupy the same site simultaneously. In one version the particles in both the tracks move counterclockwise whereas in the other version only the particles in the outer track move counter-clockwise while those in the inner track move clockwise (as shown in this figure).

$\rho_o^{cov} = r N_o/L_o$; for $r = 1$, coverage densities are identical to the corresponding particle densities.

Just as in TASEP the particles hop forward by one single lattice spacing (i.e., from one lattice site to the next on the same track) provided the target site is not covered by the leading particle. In the outer and inner tracks the hopping rates are $Q^{(o)}$ and $Q^{(i)}$, respectively provided the adjacent site on the other track is not covered by a particle; however, if the adjacent site on the other track is covered by a particle, the hopping is possible at the corresponding reduced rates $q^{(o)}$ and $q^{(i)}$, respectively. Thus, as we mentioned in the introduction, flow in the two tracks are affected by the mutual hindrance although no direct transfer of particles from one track to the other is allowed. We have studied both co-directional traffic and counter-moving traffic in the two tracks. **The figure 3 and explanation given in the figure removes any possible ambiguity in the definition of adjacency near the corners.**

Our model is very similar to the two-channel TASEP model studied by Popkov and coworkers [17, 18]. Further extension of the model by modifying the boundary conditions [19] and coupling of one-lane TASEP with a diffusive lane [20] have also been reported. However, in those two-channel TASEP models the lengths of the two channels were kept equal. In contrast, the emphasis here is on the effects of varying the ratio $f = L_i/L_o$ on the spatio-

III. RESULTS AND DISCUSSION

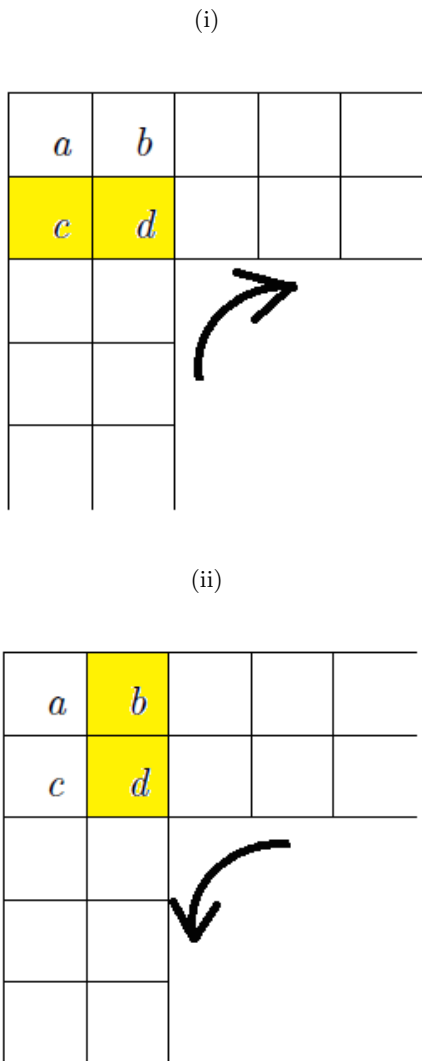


FIG. 3: Both (i) and (ii) in this figure depict only a small section of the system close to a corner. In (i) the particle at d on the inner track, while moving clockwise, finds c at a location that is continuation of its counterparts on the outer track even before it would “see” b . Therefore, in (i) the particle at d interacts with that at c , and not with b , according to the rules of the model; the particle at b on the outer track remains unaffected by that at d . In contrast, in (ii) the particle reaches d during its counter-clockwise movement on the inner track and “sees” b before it could see c . Therefore, in this case, it treats b as its counterpart on the outer track with which it interacts accordingly; the particle at c remains unaffected by that at d .

temporal organization of the particles. In fact, identifying the neighbor pairs on the two tracks, while varying f , is more straightforward in case of coaxial square tracks than in case of coaxial circular tracks.

In the following subsections, where ever possible, we provide theoretical estimates of the quantities of our interest based on either mean-field approximation or heuristic arguments. We also compute these quantities numerically by carrying out computer simulations. In order to ensure that the data are collected, indeed, in the steady state of the system we monitored the fluxes in both the tracks in our preliminary simulations. We found that, for all the system sizes and densities of our interest, the steady state is attained long before five million time steps. Therefore, for the computation of steady-state properties we discard the data for the first *five million* time steps. Throughout this paper we consider the limits $L_o \rightarrow \infty$. So far as the inner track is concerned, we’ll pay special attention to the two limits $L_i \rightarrow 0$ and $L_i \rightarrow \infty$, in addition to more general cases. Our primary interest will be the flux J_o in the outer track although we’ll also present the results for the inner track. The three main characteristic parameters of the inner track that control the nature of the flux J_o in the outer track are (i) the length L_i , (ii) the density ρ_i , and (iii) $q^{(o)}$ which is a measure of the strength of the hindrance created by the inner-track particles for the outer-track flow (and, vice-versa).

A. L_i comparable to L_o

In order to test the validity and accuracy of the approximate analytical expressions that we derive here for J_o and J_i , we also collect corresponding numerical data by direct computer simulations of the model. The chosen parameter values $L_o = 8000$ and $L_i = 7996$ not only ensure that the tracks are sufficiently long but also allow minimal difference in the lengths of the two tracks preserving their square shapes. $P_j^{(i)}$ denotes the probability of finding a particle at site j on T_i (the inner track). Similarly $P_m^{(o)}$ is the probability of finding a particle at site m on T_o (the outer track).

First we consider the simpler case of $r = 1$. In the mean-field approximation, the master equations for the probabilities $P_j^{(o)}$ and $P_j^{(i)}$ are given by

$$\begin{aligned} \frac{dP_j^{(o)}}{dt} &= [Q^{(o)}(1 - P_{j-1}^{(i)}) + q^{(o)}P_{j-1}^{(i)}] P_{j-1}^{(o)}(1 - P_j^{(o)}) \\ &\quad - [Q^{(o)}(1 - P_j^{(i)}) + q^{(o)}P_j^{(i)}] P_j^{(o)}(1 - P_{j+1}^{(o)}). \end{aligned} \quad (1)$$

$$\begin{aligned} \frac{dP_j^{(i)}}{dt} &= [Q^{(i)}(1 - P_{j-1}^{(o)}) + q^{(i)}P_{j-1}^{(o)}] P_{j-1}^{(i)}(1 - P_j^{(i)}) \\ &\quad - [Q^{(i)}(1 - P_j^{(o)}) + q^{(i)}P_j^{(o)}] P_j^{(i)}(1 - P_{j+1}^{(i)}). \end{aligned} \quad (2)$$

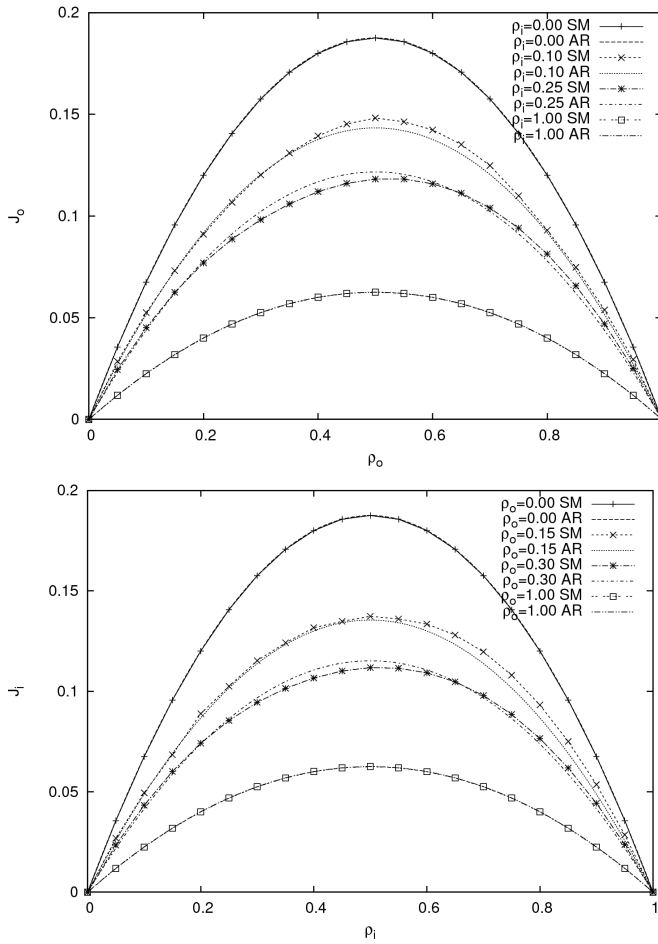


FIG. 4: (a) J_o is plotted against ρ_o for a few values of ρ_i . (b) J_i is plotted against the ρ_i for a few values of ρ_o . The discrete data points have been obtained from computer simulations of the model with parameter values $L_o = 8000$, $L_i = 7996$, $Q^{(o)} = Q^{(i)} = 0.75$ and $q^{(o)} = q^{(i)} = 0.25$. The continuous curves are obtained from the SBA outlined above with the value of μ adjusted so as to get the best fit with the simulation data.

Consequently, in the steady state the corresponding fluxes are given by

$$J_o = \omega_{mf}^{(o)} \rho_o (1 - \rho_o), \text{ and } J_i = \omega_{mf}^{(i)} \rho_i (1 - \rho_i) \quad (3)$$

where the effective hopping rates under naive mean-field approximation would be

$$\begin{aligned} \omega_{mf}^{(o)} &= Q^{(o)}(1 - \rho_i) + q^{(o)} \rho_i, \\ \omega_{mf}^{(i)} &= Q^{(i)}(1 - \rho_o) + q^{(i)} \rho_o \end{aligned} \quad (4)$$

A comparison of the mean-field predictions (3) with the corresponding simulation data revealed that the mean-field argument presented above leads to significant overestimate of both the fluxes J_o and J_i .

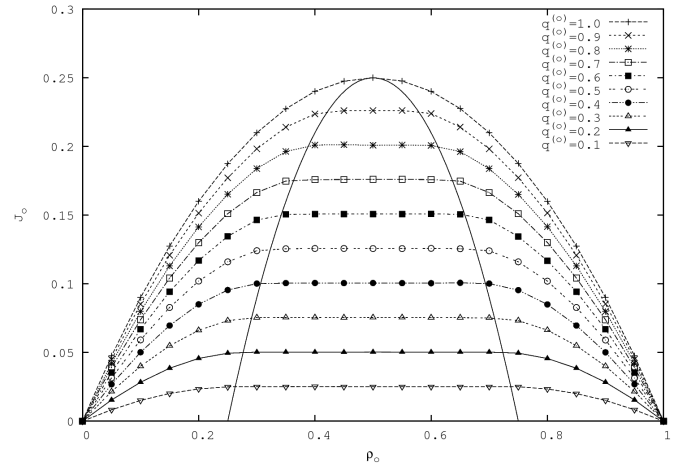


FIG. 5: J_o is plotted against ρ_o for $\rho_i = 1.0$; different curves correspond to different values of q^o . The discrete data points have been obtained from computer simulations of the model with parameter values $L_o = 8000$, $L_i = 4000$, $Q^{(o)} = 1.0$.

In order to demonstrate what happens when the ration $f = L_i/L_o$ is neither approaching zero nor approaching unity, we have plotted J_o against ρ_o in fig.5 for $L_o = 8000$, $L_i = 4000$. Since these data were generated keeping $\rho_i = 1.0$, the inner track essentially acted as an extended bottleneck against the movement of the particles in the outer track. The region under the parabola

$$J_c = \frac{1}{4} - (1 - 2\rho_c)^2 \quad (5)$$

drawn in fig.5 corresponds to the phase coexistence region. This observation is fully consistent with the theory developed earlier in ref.[8] for track-associated quenched disorder.

Our mean-field estimate could be improved by extending the concept of single-bottleneck approximation (SBA) [13, 21] that was developed for randomly distributed *static* defects on the track. If ℓ consecutive lattice sites are occupied by static defects and have defect-free sites at the two neighboring sites at the two ends of these ℓ sites, the ℓ -site ‘‘cluster’’ acts a single bottleneck of length ℓ . From the distribution of the lengths of such bottlenecks created by the independently distributed random defects one can calculate the size $\langle \ell \rangle$ of the longest bottleneck. The effect of the defects on the flux is overwhelmingly dominated by the longest bottleneck. For the purpose of our calculation we replace the probability ϕ of the presence of a static defect at a lattice site by that of a mobile particle on the neighboring track. More specifically, for the calculation of J_o we treat ρ_i as the counterpart of ϕ . Similarly, for the calculation of J_i we replace ϕ by ρ_o . Based on these heuristic arguments the fluxes J_o and J_i are given by expressions that are identical to those in (3) except that the effective hopping

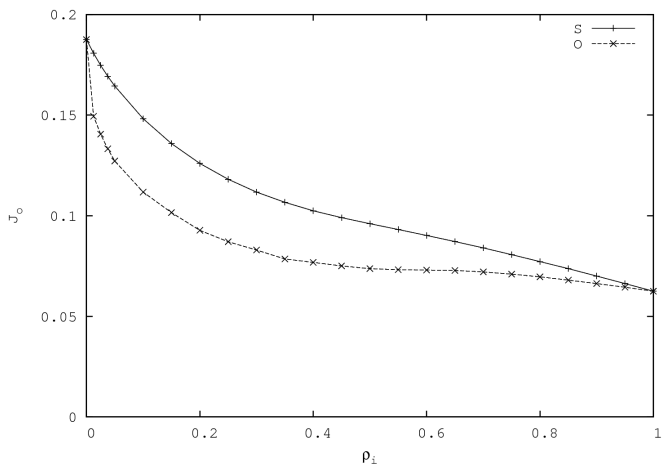


FIG. 6: Dependence of the flux on the relative direction of hopping of the particles in the two tracks is shown by plotting J_o against ρ_i for fixed $\rho_o = 0.5$. The letters ‘S’ and ‘O’ correspond to the same direction and opposite direction of flow in the two tracks. The hopping rates are $Q^{(o)} = 0.75 = Q^{(i)}$ and $q^{(o)} = 0.25 = q^{(i)}$ and the lengths of the tracks are $L_o = 8000$, $L_i = 7996$.

rates $\omega_{mf}^{(o)}$ and $\omega_{mf}^{(i)}$ are replaced by the expressions

$$\begin{aligned}\omega_{SBA}^{(o)} &= Q^{(o)} e^{-\mu \langle \ell_i \rangle} + q^{(o)} (1 - e^{-\mu \langle \ell_i \rangle}) \\ \omega_{SBA}^{(i)} &= Q^{(i)} e^{-\mu \langle \ell_o \rangle} + q^{(i)} (1 - e^{-\mu \langle \ell_o \rangle})\end{aligned}\quad (6)$$

where, utilizing the SBA [21], we have

$$\begin{aligned}\langle \ell_i \rangle &= \frac{\ln L_i + \ln(1 - \rho_i) + \gamma_e}{\ln(1/\rho_i)} - \frac{1}{2} \\ \langle \ell_o \rangle &= \frac{\ln L_o + \ln(1 - \rho_o) + \gamma_e}{\ln(1/\rho_o)} - \frac{1}{2}\end{aligned}\quad (7)$$

Note that μ is a free parameter that is varied to get the best fit with the simulation data. The best fit to the simulation data are shown in fig.4. It is worth pointing out that in spite of the increase of $\langle \ell_i \rangle$ and $\langle \ell_o \rangle$ with L_i and L_o , respectively, the exponentials in equations (6) do not vanish in the thermodynamic limit because, as we verified, μ decreases with increasing lengths of the tracks.

The magnitude of the flux J_o depends on the relative direction of motion of the particles in the two tracks. For a fixed set of parameter values, we have carried out computer simulations of the model in two different situations: (a) when particles move in the same direction in the two tracks (corresponding data are labelled by the letter ‘S’ in fig.6), and (b) when the particles move in opposite directions in the two tracks (corresponding data are labelled by the letter ‘O’ in fig.6). J_o is higher in case of co-directional motion than that for counter-directional motion on the two tracks. This difference is caused by the phase segregation of the particles into high-density and low-density regions. In case of opposite movements on the two tracks, a particle on the outer track has to

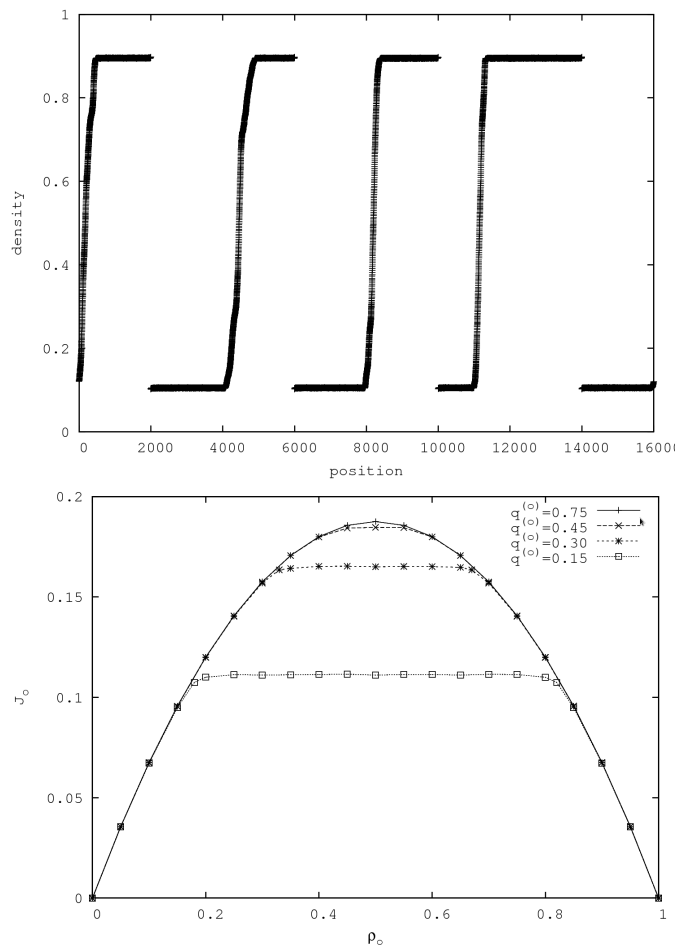


FIG. 7: (a) The density profile on the outer track for $\rho_i = 1.0$, $\rho_o = 0.5$, $Q^{(o)} = 0.9$, $q^{(o)} = 0.1$. (b) J_o is plotted against ρ_o at $\rho_i = 1.0$ for $Q^{(o)} = 0.75$ and a few different values of the parameter $q^{(o)}$. For both (a) and (b) the lengths of the tracks are $L_o = 16000$, $L_i = 4$.

overcome the full length of a high-density region on the inner track whereas the same particle need not face the full stretch of the same region if it moves co-directionally with the inner-track particles.

B. L_i vanishingly small compared to L_o

Since $L_o \rightarrow \infty$ and, since in this section we are assuming $L_i \rightarrow 4$ (the smallest allowed value of T_i that preserves its shape is 4), the inner track effectively acts as a “point” defect for the particles moving on the outer track.

First let us consider the special case $\rho_i = 1$. In this case the inner track acts effectively as a static “point-like” defect. It is well known that macroscopic phase segregation takes place in a TASEP with a single point defect, where the density profile exhibits coexistence of a high-density and low-density regimes. Since each of the

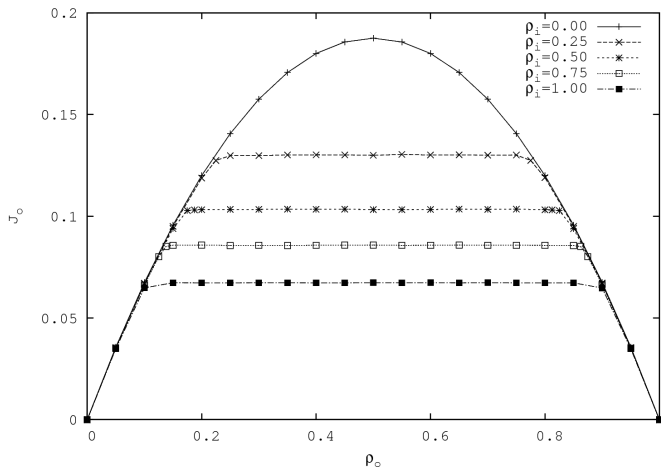


FIG. 8: J_o is plotted against ρ_o for several different values of ρ_i . The values of the other parameters used for this figure are $L_o = 8000$, $L_i = 80$, $Q^{(o)} = 0.75 = Q^{(i)}$, $q^{(o)} = 0.25 = q^{(i)}$.

four sides of the outer track in our model sees a point-like defect, the profile consists of four segments each of which is similar to that of a TASEP with a single point-defect (see fig.7). The flat symmetric plateaus observed on the plots of J_o against ρ_o correspond to the coexistence of the high-density and low-density regimes. This qualitatively similar to the corresponding flux-density diagrams for TASEPs with point defects. Moreover, as shown also in the fig.7, lower is the value of $q^{(o)}$, the stronger is the effect of the bottleneck and the smaller is the flux J_o .

Next, in order to demonstrate the more general situations, in fig.8 we have plotted J_o as a function of ρ_o for five values of the parameter $\rho_i = 0.0, 0.25, 0.5, 0.75, 1.0$. As the data in this figure show, the higher is the density ρ_i , longer is longest bottleneck and, consequently, the wider is the plateau region. This is consistent with the fact that a single bottleneck of longer size lowers the flux to a small value [2]. Finally, as expected intuitively, the flux-density curve for the outer track approaches the parabolic form $Q^o \rho_o (1 - \rho_o)$ in the limit $\rho_i \rightarrow 0$.

C. Flux-density relation for particles of size $r > 1$

Keeping in mind the possible future application of extensions of our model to the biophysical phenomena mentioned in the introduction, we have also studied the model for particle size r larger than 1. As a typical example, the flux J_o is plotted against the corresponding coverage density ρ_o^{cov} in fig.9 in those situations where

all the particles on both the tracks have the same length $r = 30$. The plateau observed in the special case $r = 1$ survives also for all $r > 1$. However, as is well known for TASEP with hard rods [2, 3], the maximum of the flux shifts to increasingly higher densities with increasing r .

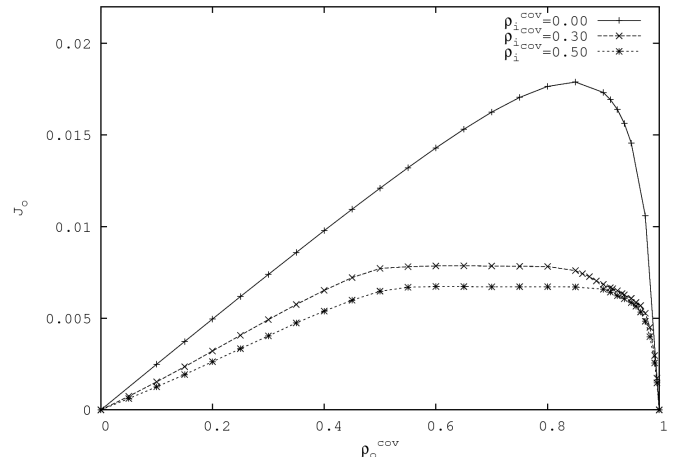


FIG. 9: J_o of particles with $r = 30$ is plotted against ρ_o^{cov} for three different values of ρ_i^{cov} ; the hopping rates are $Q^{(o)} = 0.75 = Q^{(i)}$ and $q^{(o)} = 0.25 = q^{(i)}$.

IV. SUMMARY AND CONCLUSIONS

In this paper we have developed a **simple** model for the TASEP on two co-axial square tracks that influence each other without any transfer of particles from one to another. In spite of its extreme simplicity, the model exhibits rich variety of phenomena in different parameter regimes. In the limit $L_i/L_o \rightarrow 0$, the model reproduces the known properties of a TASEP with a single “point-like” defect on the track. In particular, it exhibits macroscopic phase segregation of the particles on the outer track. In general, our model the width of the coexistence region can be tuned by varying three distinct control parameters which we have clearly identified. Extensions of this model, incorporating further details, are likely to find use in modeling the traffic-like collective biological phenomena mentioned in section II.

ACKNOWLEDGEMENTS

This work is supported by a KVPY Fellowship (SS) and a J.C. Bose National Fellowship (DC).

-
- [1] G. Schütz, in: *Phase Transitions and Critical Phenomena*, eds. C. Domb and J.L. Lebowitz (2000).
 [2] D. Chowdhury, L. Santen and A. Schadschneider, Phys.

Rep. **329**, 199 (2000).

- [3] A. Schadschneider, D. Chowdhury and K. Nishinari, *Stochastic transport in complex systems: from molecules*

- to vehicles*, (Elsevier, 2010).
- [4] D. Chowdhury, A. Schadschneider and K. Nishinari, *Phys. of Life Rev.* **2**, 318 (2005).
 - [5] T. Chou, K. Mallick and R.K.P. Zia, *Rep. Prog. Phys.* **74**, 116601 (2011).
 - [6] D. Chowdhury, *Phys. Rep.* **529**, 1 (2013).
 - [7] S.A. Janowsky and J.L. Lebowitz, *Phys. Rev. A* **45**, 618 (1992); *J. Stat. Phys.* **77**, 35 (1994).
 - [8] G. Tripathy and M. Barma, *Phys. Rev. Lett.* **78**, 3039 (1997); *Phys. Rev. E* **58**, 1911 (1998).
 - [9] R.J. Harris and R.B. Stinchcombe, *Phys. Rev. E* **70**, 016108 (2004).
 - [10] J. Krug and P. A. Ferrari, *J. Phys. A* **29**, L465 (1996)
 - [11] M. R. Evans, *Europhys. Lett.* **36**, 13 (1996); *J. Phys. A* **30**, 5669 (1997).
 - [12] D. Ktitarev, D. Chowdhury and D. Wolf, *J. Phys. A* **30**, L221 (1997).
 - [13] J. Krug, *Braz. J. Phys.* **30**, 97 (2000).
 - [14] A.B. Kolomeisky, *J. Phys. Condens. Matt.* **25**, 463101 (2013).
 - [15] A. Helmrich, M. Ballarino, E. Nudler and L. Tora, *Nat. Struct. Mol. Biol.* **20**, 412 (2013).
 - [16] B.J. Brewer, *Cell* **53**, 697 (1988).
 - [17] V. Popkov and I. Peschel, *Phys. Rev. E* **64**, 026126 (2001).
 - [18] V. Popkov and G.M. Schütz, *J. Stat. Phys.* **112**, 523 (2003).
 - [19] A. Melbinger, T. Reichenbach, T. Franosch and E. Frey, *Phys. Rev. E* **83**, 031923 (2011).
 - [20] M.R. Evans, Y. Kafri, K.E.P. Sugden and J. Tailleur, *J. Stat. Mech. Theor. Expt.* P06009 (2011).
 - [21] P. Greulich and A. Schadschneider, *J. Stat. Mech: Theor Expt.*, P04009 (2008).